Received: 15 June 2020 | Revised: 28 February 2021 | Accepted: 10 May 2021

DOI: 10.1002/joc.7198

RESEARCH ARTICLE

International Journal of Climatology RMetS

The impact of coupled air–sea interaction on extreme East Asian summer monsoon simulation in CMIP5 models

Taehyung Kim[1] | **Soheon Lee**[1] | **Hye-Jin Park**[1] | **Dong-Hyun Cha**[1] | **Kyong-Hwan Seo**[2]

[1]School of Urban and Environmental Engineering, Ulsan National Institute of Science and Technology, Ulsan, South Korea

[2]Department of Atmospheric Sciences, Pusan National University, Busan, South Korea

Correspondence
Dong-Hyun Cha, School of Urban and Environmental Engineering, Ulsan National Institute of Science and Technology, 50 UNIST-gil, Eonyang-eup, Ulju-gun, Ulsan 689-798, South Korea.
Email: dhcha@unist.ac.kr

Funding information
Research and Development; Korea Meteorological Administration

Abstract

In this study, the relationship between the ability to simulate air–sea interactions over the western North Pacific (WNP), and to reproduce the extreme East Asian summer monsoon (EASM), were investigated by comparing the performances of several global climate models (GCMs). High ranked in air–sea interaction simulation (HRA) and low ranked in air–sea interaction simulation (LRA) models were selected, according to their performance in simulating relations between sea surface temperature (SST) and precipitation over the WNP, from the ensemble of models that participated in the third and fifth phases of the Coupled Model Intercomparison Project (CMIP3, CMIP5). Compared with CMIP3 models, CMIP5 models exhibited improved simulations of the distinctive air–sea interaction over the WNP, namely, the strong atmospheric forcing on the ocean. Among CMIP5 models, HRA models, which reproduced intrinsic negative correlations between precipitation and SST over the WNP, could simulate the extreme EASM better than LRA models. In particular, HRA models generated a more realistic spatial distribution of the extreme EASM compared with LRA models. The defects of the LRA models resulted from distorted synoptic fields, including underestimated geopotential height and overestimated low-level wind over the WNP, inducing unrealistic moisture supply and convection due to the exaggerated SST forcing. In contrast, reasonable air–sea interactions represented in HRA models lead to realistic synoptic fields over the WNP, and proper simulation of the extreme EASM.

KEYWORDS

air–sea interaction, coupled model Intercomparison project, East Asian summer monsoon

1 | INTRODUCTION

Monsoon circulation is a distinct climate phenomenon caused by thermal differences between continents and oceans and affects regional climate circulation worldwide. The East Asian summer monsoon (EASM) is an especially critical component of East Asia's general circulation system (Lau *et al*., 2000). The EASM is a broad-scale summer monsoon over East Asia and the western North Pacific (WNP). It covers China, Korea, Japan, and surrounding ocean basins. The extreme EASM is often accompanied by various extreme weather events, including heat waves, drought, and heavy rainfall, or floods, which lead to significant social, economic, and environmental damage. Therefore, accurate models for the simulation of extreme EASM are required for proper

preparedness for the disasters caused by high-impact weather and climate events. A noticeable feature of this monsoon system is the broad range of duration, areal extent, and intensity of precipitation across different events. In particular, the rainband associated with the EASM generally develops over the Eurasian continent as well as the WNP. Associated with the formation of the rainband over the ocean, although recent studies stress the importance of the Tibetan plateau-driven surface heating (Wu *et al*., 2012) and topographically forced downstream Rossby waves and resulting southerly moist wind (Son *et al*., 2019), air–sea interaction is another major factor to be considered (Tompkins, 2001). This two-tier energy exchange between the atmosphere and the ocean indicates that the ocean not only controls atmospheric conditions but is, in turn, affected by the atmosphere.

Air–sea interactions can be explained by the relationship between sea surface temperature (SST) and precipitation. SST plays a crucial role in driving atmospheric processes when SST anomalies are large. A warm SST anomaly in the tropics and subtropics can increase convective activities and regional precipitation. Thus, precipitation tends to be positively correlated with SST anomalies. In contrast, negative correlations between precipitation and SST anomalies can exist if the impact of the atmosphere on SST is greater than the forcing exerted by SST on the atmosphere; increased clouds and precipitation can decrease insolation and increase ocean boundary layer mixing, leading to a negative SST anomaly (Wang *et al*., 2005; Cha *et al*., 2016) and the correlation between precipitation and SST anomaly may be negative. The WNP, often called the 'western Pacific warm pool', differs from other ocean basins in having a unique characteristic regarding the SST–precipitation relationship. Tompkins (2001) demonstrated that SST observed over the WNP appears to be inversely proportional to precipitation, implying that atmospheric conditions determine oceanic activity, even with remarkably high SSTs of ~30°C. If simulated SST does not change as a function of simulated precipitation and low-level wind, unreasonable positive feedbacks between the sea surface and precipitation will lead to unrealistic simulations of the extreme EASM (Cha *et al*., 2016). Therefore, the objectives of this study were to evaluate the abilities of a number of global climate models (GCMs) to simulate air–sea interactions and to investigate the impact of these abilities on the accuracy of simulations of the extreme EASM.

The lack of accurate simulation of these aspects of air–sea interaction in GCMs can be related to numerous errors in forecasting atmospheric phenomena. Global climate models that were included in the atmospheric model intercomparison project (AMIP) produced unrealistic variability in precipitation associated with the Asian–Pacific summer monsoon. One reason for the failure was the neglect of air–sea interactions in the warm Indo–Pacific oceans (Gadgil and Sajani, 1998). Air–sea interactions are especially different for the WNP, making this a particularly critical error. Wang *et al*. (2005) demonstrated that a major cause of rainfall-deficiencies in atmospheric general circulation models (AGCMs) is the absence of consideration of atmospheric feedback to the oceans. Due to its importance, air–sea interaction is of interest to many scientists. Various studies have demonstrated that the performance of GCMs and regional climate models (RCMs) could be improved when ocean models are coupled. For example, the air–sea coupled system allows more realistic simulation than the atmosphere-only approach for the boreal-summer intraseasonal oscillation (BSISO) and climatological intraseasonal oscillation (CISO) of the mean Asian summer monsoon (Fu *et al*., 2002; Fu and Wang, 2004; Seo *et al*., 2007). Similarly, for RCMs, the implementation of an ocean mixed layer model into the Weather Research and Forecasting (WRF) model tended to improve simulations of the summer climate over East Asia during 2000–2008 (Kim and Hong, 2010). This was because the ocean model cooled down SST and stabilized the thermodynamic structure near the surface, reducing the previously overestimated summer precipitation, and weakened the sub-tropical high. Zou and Zhou (2013), Zou and Zhou (2014) and Zou *et al*. (2016) proved that a Flexible Regional Ocean–Atmosphere-Land surface-Sea ice coupled model (FROALS), which consists of the Regional Climate Model, version 3 (RegCM3), and the National Key Laboratory of Numerical Modelling for Atmospheric Sciences and Geophysical Fluid Dynamics (LASG)/Institute of Atmospheric Physics (IAP) Climate System Ocean Model (LICOM) tended to improve the simulation of the EASM climatology and interannual variability. Cha *et al*. (2016) also demonstrated that runs of the Seoul National University regional climate model (SNURCM) coupled with a slab ocean model (SOM) represented western North Pacific subtropical high (WNPSH), seasonal mean rainfall, and monsoon circulations more realistically than uncoupled runs.

The Coupled Model Intercomparison Project (CMIP) was established to study and inter-compare climate representations made using coupled ocean–atmosphere–cryosphere–land GCMs (Meehl *et al*., 2000). Song and Zhou (2014b) demonstrated that Coupled GCMs have better skills than those of AGCMs in the EASM simulation in both climatology and inter-annual variability. As coupled GCMs have been upgraded and the version numbers of the models participating in each phase have advanced, their performances have improved, compared

with earlier versions of the models. For example, climatological seasonal means and inter-annual standard deviations of precipitation simulated by the global models participating in the fifth phase of the Coupled Model Intercomparison Project (CMIP5) was significantly improved compared with those simulated by the third phase (CMIP3) models (Seo *et al*., 2013). Nevertheless, comparisons of representations of air–sea interactions over the WNP between CMIP5 and CMIP3 models are yet to be investigated. In addition, specific evaluations of the SST–precipitation relationship over the WNP, where the SST–precipitation correlation is most strongly negative, are yet to be documented (Lu and Lu, 2014). Moreover, the impact of air–sea interaction on the simulation of the extreme EASM should be analyzed more deeply. Therefore, the aims of this study are to examine how simulations of air–sea interactions over the WNP improve in CMIP5 models and to investigate their impact on simulations of the extreme EASM.

Section 2 describes the data used in this study. In Section 3, comparisons of model performance in reproducing WNP Air–Sea interaction Index (ASI), between CMIP5 and CMIP3, are described, and the relationship between CMIP5 model performances simulating WNP ASI and the reproduction of the extreme EASM years is investigated. Finally, Section 4 presents the summary and conclusion.

2 | MODELS, DATA SETS, AND METHODS

A large ensemble of GCM data were selected from the 'Climate of the 20th century' experiment of the World Climate Research Programme (WCRP) CMIP3 (Meehl *et al*., 2007), and from the historical multi-model data sets from WCRP CMIP5 (Taylor *et al*., 2012). The available model outputs are from 20 models of CMIP3 and 44 models of CMIP5 (Table 1), and one realization (run 1 for CMIP3 and r1i1p1 for CMIP5) of each GCM was taken into account. Monthly SST, precipitation, geopotential height, and zonal and meridional winds produced by these models were used for analysis. Observational and reanalysis data sets used in this study consisted of the following: (a) the Global Precipitation Climatology Project (GPCP) (Adler *et al*., 2003) for monthly and daily precipitation data; (b) Extended Reconstructed SST data version 5 for monthly SST data (Huang *et al*., 2017); (c) the National Centers for Environmental Prediction/Department of Energy (NCEP/DOE) R-2 data (Kanamitsu *et al*., 2002) for geopotential height and wind. All data sets were converted into a common grid with 2.5° × 2.5° resolution. The analysis period of all models and observational data used in this study was

TABLE 1 (a) CMIP3 and (b) CMIP5 model list and their corresponding institutions

(a) CMIP3	
Models	**Institution**
BCCR-BCM2.0	Bjerknes Centre for Climate Research
CNRM-CM3	Météo-France/Centre National de Recherches Météorologiques
CSIRO-Mk3.0	Commonwealth Scientific and Industrial Research Organization Atmospheric Research
ECHO-G	Meteorological Institute of the University of Bonn, Meteorological Research Institute of KMA and Model and Data group
FGOALS-g1.0	LAGS/Institute of Atmospheric Physics
GFDL-CM2.0	US Department of Commerce/NOAA/Geophysical Fluid Dynamics Laboratory
GFDL-CM2.1	US Department of Commerce/NOAA/Geophysical Fluid Dynamics Laboratory
GISS-AOM	NASA/Goddard Institute for Space Studies
GISS-EH	NASA/Goddard Institute for Space Studies
GISS-ER	NASA/Goddard Institute for Space Studies
UKMO-HadCM3	Hadley Centre for Climate Prediction and Research/Met Office
UKMO-HadGEM1	Hadley Centre for Climate Prediction and Research/Met Office
INM-CM3.0	Institute for Numerical Mathematics
IPSL-CM4	Institut Pierre-Simon Laplace
MIROC3.2 (hires)	Center for Climate System Research (The University of Tokyo), National Institute for Environmental Studies, and Frontier Research Center for Global Change (JAMSTEC)
MIROC3.2 (medres)	Center for Climate System Research (The University of Tokyo), National Institute for Environmental Studies, and Frontier Research Center for Global Change (JAMSTEC)
ECHAM5/MPI-OM	Max Planck Institute for Meteorology
MRI-CGCM2.3.2	Meteorological Research Institute
CCSM3	National Center for Atmospheric Research
PCM	National Center for Atmospheric Research
(b) CMIP5	
Models	**Institution**
ACCESS1.0	CSIRO (Commonwealth Scientific and Industrial Research Organisation, Australia), and BOM (Bureau of Meteorology, Australia)
ACCESS1.3	CSIRO (Commonwealth Scientific and Industrial Research Organisation, Australia), and BOM (Bureau of Meteorology, Australia)
BCC-CSM1.1	Beijing Climate Center, China Meteorological Administration

(Continues)

TABLE 1 (Continued)

(b) CMIP5	
Models	**Institution**
BCC-CSM1.1 (m)	Beijing Climate Center, China Meteorological Administration
CanCM4	Canadian Centre for Climate Modeling and Analysis
CanESM2	Canadian Centre for Climate Modeling and Analysis
CCSM4	National Center for Atmospheric Research
CESM1-BGC	National Science Foundation, Department of Energy, National Center for Atmospheric Research
CESM1-CAM5	National Science Foundation, Department of Energy, National Center for Atmospheric Research
CESM1-FASTCHEM	National Science Foundation, Department of Energy, National Center for Atmospheric Research
CESM1-WACCM	National Science Foundation, Department of Energy, National Center for Atmospheric Research
CMCC-CESM	Centro Euro-Mediterraneo per I Cambiamenti Climatici
CMCC-CM	Centro Euro-Mediterraneo per I Cambiamenti Climatici
CMCC-CMS	Centro Euro-Mediterraneo per I Cambiamenti Climatici
CNRM-CM5	Centre National de Recherches Meteorologiques/Centre Europeen de Recherche et Formation Avancees en Calcul Scientifique
CSIRO-Mk-3-6-0	Commonwealth Scientific and Industrial Research Organisation in collaboration with the Queensland Climate Change Centre of Excellence
FGOALS-g2	LASG, Institute of Atmospheric Physics, Chinese Academy of Sciences, and CESS, Tsinghua University
FIO-ESM	The First Institute of Oceanography, SOA, China
GFDL-CM2.1	Geophysical Fluid Dynamics Laboratory
GFDL-CM3	Geophysical Fluid Dynamics Laboratory
GFDL-ESM2G	Geophysical Fluid Dynamics Laboratory
GFDL-ESM2M	Geophysical Fluid Dynamics Laboratory
GISS-E2-H-CC	NASA Goddard Institute for Space Studies
GISS-E2-H	NASA Goddard Institute for Space Studies
GISS-E2-R-CC	NASA Goddard Institute for Space Studies
GISS-E2-R	NASA Goddard Institute for Space Studies
HadCM3	Met Office Hadley Centre
HadGEM2-AO	Met Office Hadley Centre
HadGEM2-CC	Met Office Hadley Centre
HadGEM2-ES	Met Office Hadley Centre
INMCM4	Institute for Numerical Mathematics
IPSL-CM5A-LR	Institut Pierre-Simon Laplace
IPSL-CM5A-MR	Institut Pierre-Simon Laplace
IPSL-CM5B-LR	Institut Pierre-Simon Laplace
MIROC4h	Atmosphere and Ocean Research Institute (The University of Tokyo), National Institute for Environmental Studies, and Japan Agency for Marine-Earth Science and Technology
MIROC5	Atmosphere and Ocean Research Institute (The University of Tokyo), National Institute for Environmental Studies, and Japan Agency for Marine-Earth Science and Technology
MIROC-ESM	Atmosphere and Ocean Research Institute (The University of Tokyo), National Institute for Environmental Studies, and Japan Agency for Marine-Earth Science and Technology
MIROC-ESM-CHEM	Atmosphere and Ocean Research Institute (The University of Tokyo), National Institute for Environmental Studies, and Japan Agency for Marine-Earth Science and Technology
MPI-ESM-LR	Max Planck Institute for Meteorology
MPI-ESM-MR	Max Planck Institute for Meteorology
MPI-ESM-P	Max Planck Institute for Meteorology
MRI-CGCM3	Meteorological Research Institute
NorESM1-M	Norwegian Climate Centre
NorESM1-ME	Norwegian Climate Centre

Note: Further information on the models used can be obtained from https://pcmdi.llnl.gov/mips/.

from 1980 to 1999, and the summer seasonal mean of June to August (JJA) was used. To evaluate the ability of GCMs, an Air–Sea interaction index (ASI), defined as the simultaneous correlation coefficient between precipitation and SST anomaly, was applied in this study. Simultaneous correlation coefficients between summer mean precipitation and SST anomaly (also referred to as the ASI) were calculated from 1980 to 1999 to analyze air–sea interactions over the WNP and to compare the capability of the ASI simulation in CMIP3 and CMIP5.

To examine the overall performance of CMIP3 and CMIP5 models, the Taylor (2001) analysis was performed for simulated versus observed ASI. The Taylor skill score S is defined as:

$$S=\frac{4(1+R)}{\left(\hat{\sigma}_f+1/\hat{\sigma}_f\right)^2(1+R_0)},$$

where R is the spatial correlation between simulated and observed values, $\hat{\sigma}_f$ is the ratio of simulated and observed standard deviation (SD), and R_0 is the maximum possible correlation (here set to 1). The skill score S, therefore, can simultaneously evaluate both the normalized spatial standard deviation and pattern correlation. According to the ASI-reproducing skill score, good-performing in air–sea interaction and poor-performing in air–sea interaction models were selected and compared.

3 | RESULTS

3.1 | Comparison of the performances of the models in simulating air–sea interactions over the WNP: CMIP3 versus CMIP5

The ASI reproduced by GCMs participating in CMIP3 and CMIP5 are analyzed in this section. To understand air–sea interactions over the WNP, observed ASI is analyzed in Figure 1a, where negative ASI is observed to be dominant in most regions of the WNP. Prominent negative ASI was apparent not only in the mid-latitudes around the Korean peninsula (~30°N) but also in tropical regions near the Philippines. Near the South China Sea (SCS) and over the Philippine Sea, a core region (10–30°N, 110–135°E) with strong negative ASI, where the correlation coefficient between precipitation and SST anomaly was lower than −0.6, were particularly apparent. The impact of the atmosphere on the ocean is stronger than the oceanic forcing on the atmosphere in this region. This negative ASI was then reversed to positive in the central Pacific above 160°E (not shown). To compare the performance of 20 CMIP3 models and 44 CMIP5 models in simulating air–sea interactions over the WNP, ASI from each model was calculated and compared with the observed ASI (Figure 1b,c). The averaged result of 20 models from CMIP3 did not realistically represent the intrinsic air–sea interaction (Figure 1b); the ASI over the core region with large negative ASI, as well as the SCS, was dominated by a near-zero signal rather than the observed strong negative signal. This result can be attributed to the fact that the GCMs rarely accurately simulated the observed relationship between precipitation and SST over the WNP. Possible reasons why CMIP3 models failed to simulate the air–sea interaction over the WNP might be: (a) atmospheric motion, such as convection, was too sensitive to SST in models; and (b) declines in SST arising from precipitation and cloud cover remain poorly simulated. Compared with results obtained through CMIP3, the CMIP5 ensemble exhibited a more reasonable distribution of ASI (Figure 1c). In particular, negative ASI over the SCS was captured to some extent, with a value of −0.2. In addition, the root-mean-square error (RMSE) of the CMIP5 ensemble (0.37) was smaller than that of the CMIP3 ensemble (0.43), indicative of an improved simulation of air–sea interactions over the WNP in CMIP5 models compared with CMIP3 models. CMIP5 ensemble results, however, remain far from accurate. Air–Sea interaction index signals were mostly too weak over the WNP, and relatively high positive ASI occurred near the equator.

To clarify whether CMIP5 models were better at simulating air–sea interactions over the WNP after revisions from CMIP3, models with good performance in air–sea interaction and models with poor performance in air–sea interaction were selected based on their ability to accurately simulate ASI. Figure 2 shows the Taylor skill score S for ASI, calculated from the CMIP3 and CMIP5 models output, in ascending order. Models with a standard deviation of higher (lower) than + (−) 1σ of the Taylor skill scores between the models were selected as HRA (LRA) models. From this criterion, five HRA models (GISS-ER, UKMO-HadGEM1, MIROC3.2 [hires], GFDL-CM2.0, and ECHO-G) and five LRA models (FGOALS-g1.0, CNRM-CM3, PCM, MRI-CGCM2.3.2, and CSIRO-Mk3.0) were identified in CMIP3. Similarly, eight HRA models (CESM1-CAM5, CCSM4, CNRM-CM5, MIROC-ESM-CHEM, MIROC4h, CMCC-CMS, MRI-CGCM3, MIROC-ESM) and six LRA models (CSIRO-Mk3-6-0, CMCC-CESM, ACCESS1-3, IPSL-CM5A-LR, GISS-E2-H-CC, CMCC-CM) were adopted from CMIP5. As a result, the skill score of the ensemble of the CMIP3 HRA models was 0.61, and that of the ensemble of the CMIP3 LRA models was 0.42. In addition, the skill score of the ensemble of CMIP5 HRA models was 0.65, and that of the ensemble of CMIP5 LRA models was 0.42.

Figure 3 shows the averaged ASI from the HRA and LRA models from CMIP3 and CMIP5. In both CMIP3 and CMIP5, the ensemble of LRA models showed that precipitation tended to increase as SST increased (i.e., positive ASI) in most areas in the WNP (Figure 3a,b). This implies that the response of precipitation to SST change in the WNP is stronger than the response of SST to changes of rainfall and synoptic-scale atmospheric conditions; warmer SST forcings increase precipitation, but changes of rainfall and synoptic-scale atmospheric condition cannot cool SST. This is also supported by the strong ASI (> 0.4) near the equator because the higher SST can trigger more convective precipitation (Figure 3a). The notable difference in the ensemble of LRA models, between CMIP3 and CMIP5, was the sign of ASI in the SCS. Only some LRA models of CMIP5 showed positive ASI in the SCS whereas all LRA models of CMIP3 showed positive ASI. In contrast, the ensembles of HRA models from CMIP3 and CMIP5 exhibited more examples of negative ASI in the SCS, the Philippine Sea, and coasts in East Asia (the East China Sea and around the Korean peninsula and Japan) than the

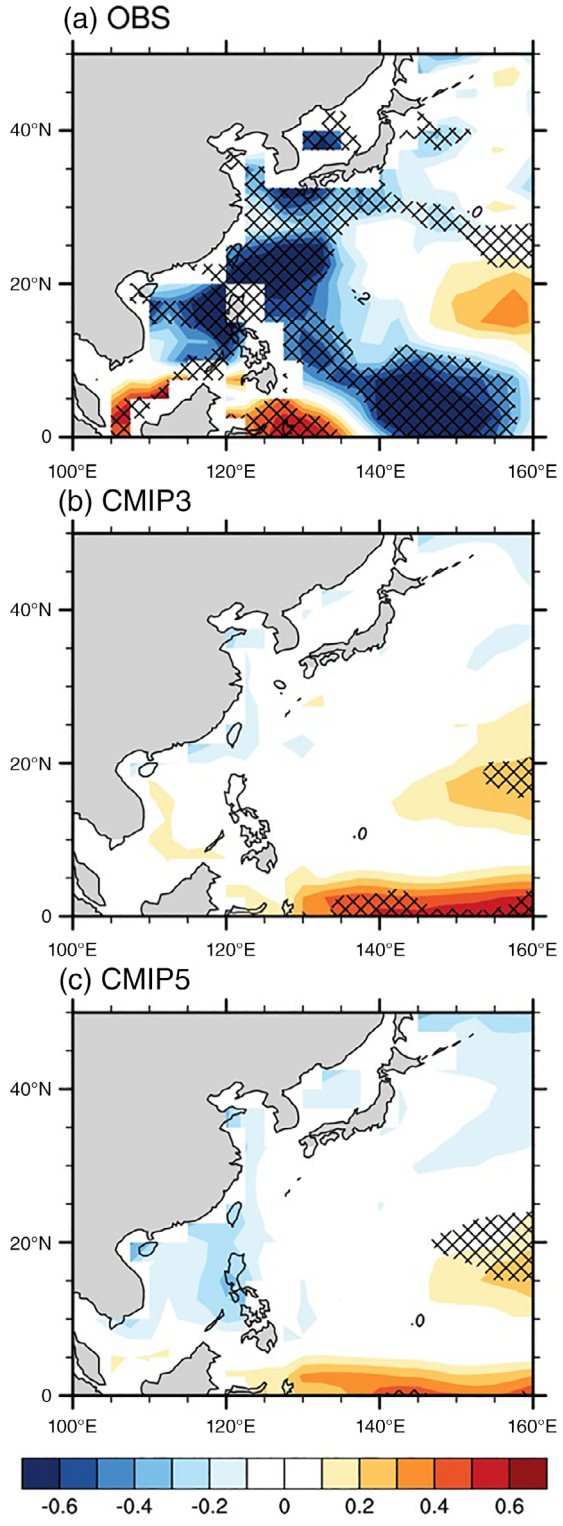

FIGURE 1 ASI in (a) observation, (b) CMIP3 ensemble and (c) CMIP5 ensemble for the boreal summer (JJA) from 1980 to 1999. The ASI in observation is the simultaneous correlation coefficients between the precipitation from GPCP and sea surface temperature from ERSST. The simulated ASIs were calculated by the multi-model ensemble simulation of 20 CMIP3 models and 44 CMIP5 models, respectively. Dashed line indicate the areas where the correlation coefficients are significant at the 90% confidence level [Colour figure can be viewed at wileyonlinelibrary.com]

ensembles of LRA models (Figure 3c,d). The negative correlation between precipitation and SST anomaly over the core region (10–30°N, 110–135°E) of the WNP in the ensemble of HRA models was much closer to the observed correlation, compared with the ensembles of LRA models. HRA models of CMIP5 simulated a stronger negative ASI and exhibited a larger degree of consistency across models, compared with CMIP3 HRA models, indicating an improvement of the simulation of the air–sea interactions over the WNP. Table 2 shows the statistics (i.e., RMSE and spatial correlation) between the observed and simulated ASI from CMIP3 and CMIP5. Even the ensemble of LRA models in CMIP5 somewhat improved in both RMSE and spatial correlation. Spatial correlations of the ensemble of CMIP5 HRA models were higher than that of the ensemble

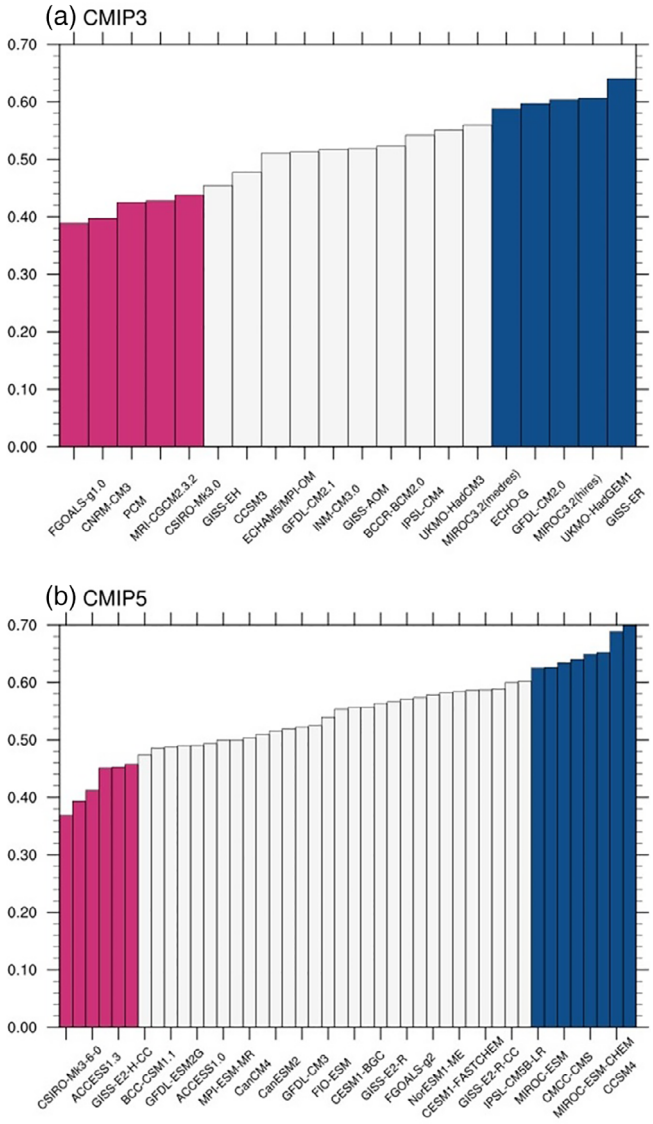

FIGURE 2 Taylor skill score of ASI calculated by (a) CMIP3 models and (b) CMIP5 models [Colour figure can be viewed at wileyonlinelibrary.com]

of CMIP3 HRA models. RMSEs calculated for the core region (denoted in parenthesis) and the analysis region as a whole were reduced in CMIP5 HRA models. This indicates that the models participating in CMIP5 were improved compared with CMIP3 models, in terms of simulating the air–sea interactions over the WNP.

3.2 | The relationship between CMIP5 model performances in simulating WNP air–sea interactions and reproduction of the extreme EASM

The previous section showed that CMIP5 models tended to exhibit improved simulation of air–sea interactions over the WNP compared with CMIP3 models. In this section, we investigate how the performance of simulated ASI would affect the reproduction of the extreme EASM through a comparison of HRA and LRA models in CMIP5.

In the summer, rainbands associated with two major monsoons (East Asian summer monsoon, EASM, and WNP summer monsoon: WNPSM) appeared over East Asia (Wang and LinHo, 2002). The EASM was characterized by rainfall across the area, including China, Korea, and Japan. The major regions with the highest rate of precipitation within the EASM were southern and central China, South Korea, and Japan. At the same time, the WNPSM was associated with heavy precipitation that was concentrated in the southern regions (i.e., the SCS

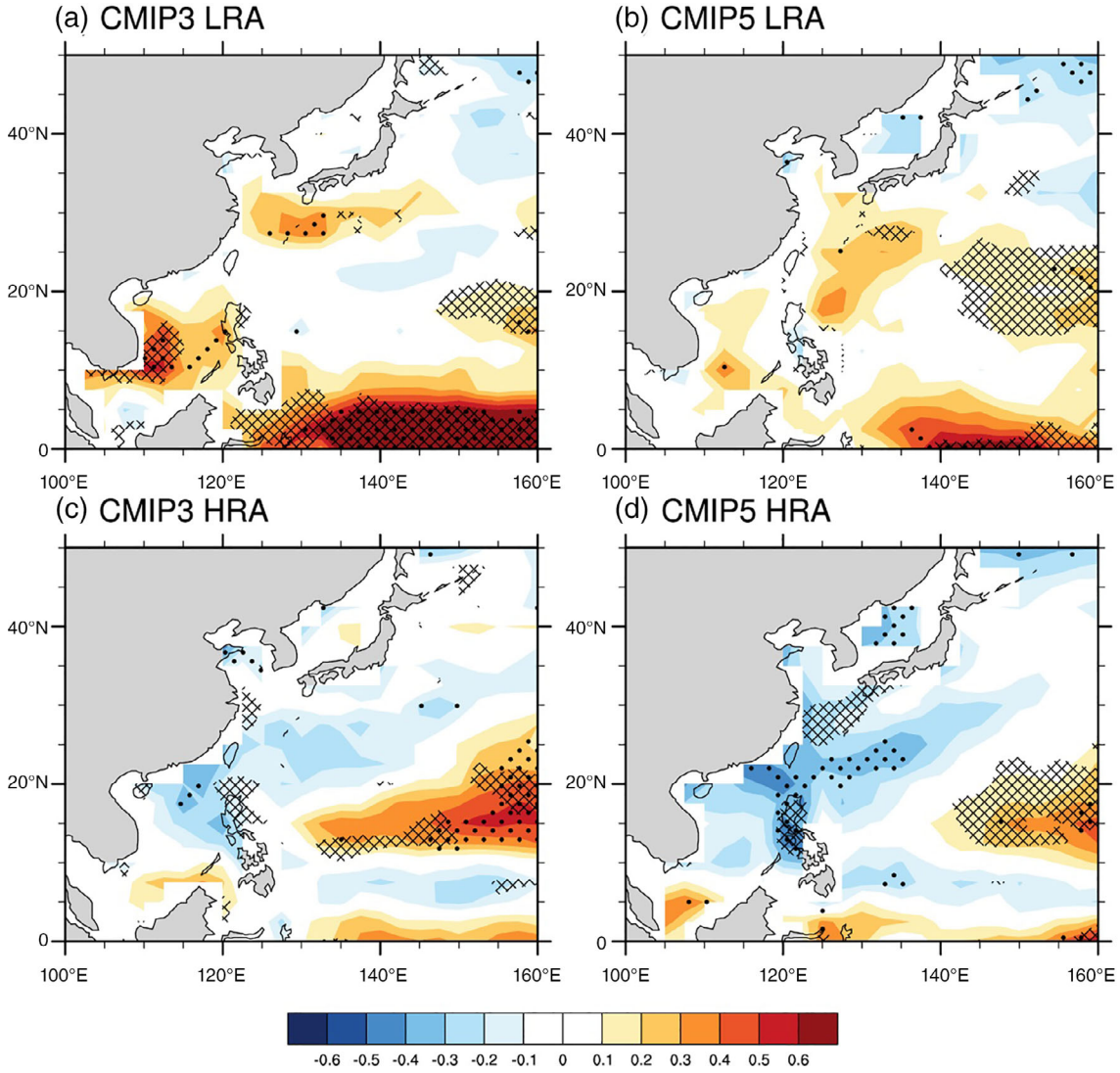

FIGURE 3 ASI produced by multi-model ensemble of (a) CMIP3 LRA models, (b) CMIP5 LRA models, (c) CMIP3 HRA models, and (d) CMIP5 HRA models. The dots denote the consistency of ASI signal between ensemble members indicating all ensemble members have same ASI signal. Dashed line indicates the areas where the correlation coefficients are significant at the 90% confidence level [Colour figure can be viewed at wileyonlinelibrary.com]

TABLE 2 Root-mean-square error (RMSE) and spatial correlation of ASI between the observation and simulations of CMIP3 and CMIP5

	CMIP3 LRA model ensemble	CMIP5 LRA model ensemble	CMIP3 HRA model ensemble	CMIP5 HRA model ensemble
RMSE	0.57 (0.62)	0.49 (0.61)	0.37 (0.41)	0.31 (0.30)
Spatial correlation	−0.22	−0.19	0.38	0.52

Note: The value in a parenthesis denote the corresponding value in the core region (10–30°N, 110–135°E).

TABLE 3 Strong and weak EASM years simulated by CMIP5 HRA and LRA model ensembles

	Model	Strong EASM years	Weak EASM years
HRA model ensemble	MIROC-ESM	1984, 1988, 1991, 1997, 1999	1980, 1981, 1982, 1983, 1987, 1993
	MRI-CGCM3	1985, 1993, 1996	1982, 1983, 1988, 1997
	CMCC-CMS	1980, 1982, 1989	1981, 1988, 1991, 1996
	MIROC4h	1992, 1995, 1997, 1998	1985, 1990, 1991, 1993, 1994
	MIROC-ESM-CHEM	1980, 1996, 1999	1984, 1985, 1987, 1988, 1992
	CNRM-CM5	1980, 1982, 1986, 1988, 1998	1981, 1987, 1989, 1990, 1991, 1993, 1997
	CCSM4	1987, 1993, 1995	1980, 1989, 1990, 1991
	CESM1-CAM5	1988, 1990, 1993, 1994, 1997, 1999	1980, 1981, 1984, 1987, 1992, 1996, 1998
LRA model ensemble	CSIRO-Mk3-6-0	1985, 1986, 1994	1980, 1984, 1987, 1992, 1993
	CMCC-CESM	1982, 1986, 1989, 1997	1983, 1984, 1990, 1992, 1998, 1999
	ACCESS1.3	1980, 1982, 1984, 1986, 1993, 1994, 1996	1981, 1985, 1989, 1990, 1992, 1999
	IPSL-CM5A-LR	1980, 1983, 1985, 1991, 1994, 1996, 1998	1982, 1988, 1990, 1992, 1993, 1995, 1997
	GISS-E2-H-CC	1981, 1985, 1989, 1991	1982, 1984, 1993
	CMCC-CM	1982, 1984, 1990, 1996	1986, 1997, 1998

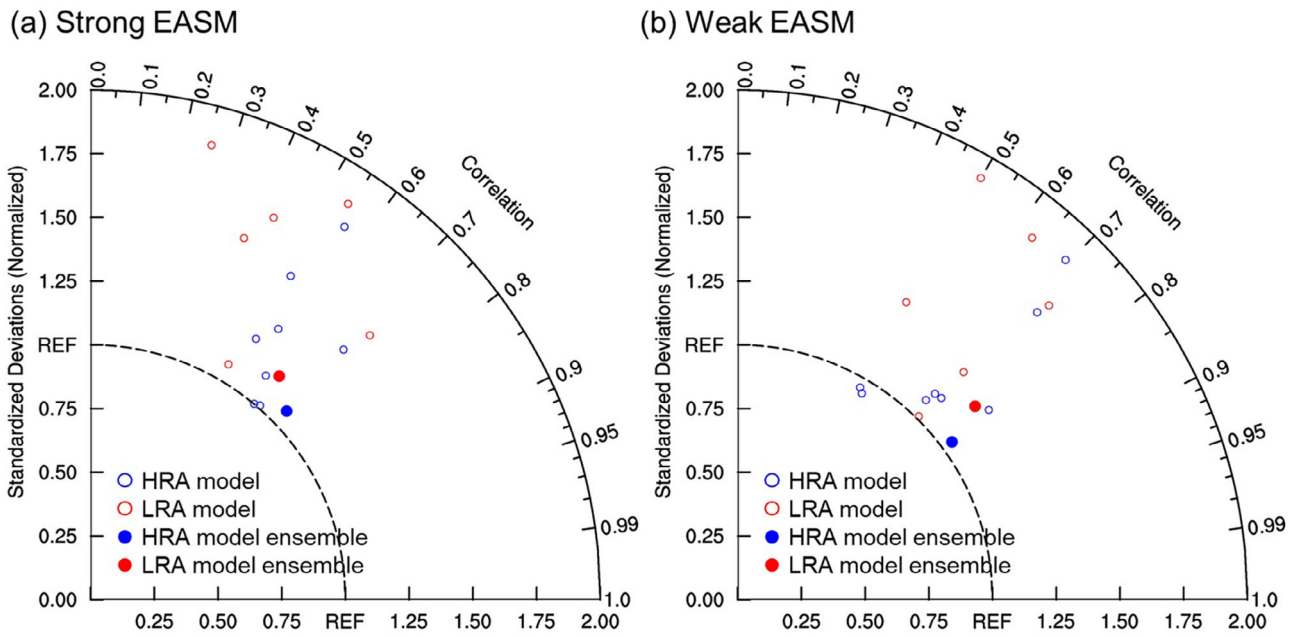

FIGURE 4 Pattern correlation coefficient and ratio of spatial *SD* of the summer (JJA) precipitations between the observation, and simulations from CMIP5 HRA models (blue) and CMIP5 LRA models (red) for the period of strong EASM years (left) and weak EASM (right) [Colour figure can be viewed at wileyonlinelibrary.com]

and over the tropical WNP), below 20°N. The area from 130 to 160°E between these summer monsoon rainbands had relatively little precipitation because of the WNPSH. This dipole mode of the EASM and WNPSM exhibits inter-annual variability (Wang *et al*., 2001; Kwon *et al*., 2005; Yim *et al*., 2008; Cha *et al*., 2011; Song and Zhou, 2014a; Song and Zhou, 2014b). Depending on their phase, extreme monsoon years can be divided into strong and weak EASM years. In each extreme case, different meteorological phenomena occur in East Asia and the WNP. In 1994, a representative of weak EASM years, there were record-breaking heat waves and drought during the summer monsoon season due to anomalous circulations over the East Asian-northwestern Pacific region and over the subtropical western Pacific (Park and Schubert, 1997). In contrast, 1991 and 1998 are examples of strong EASM years. There were heavy precipitation events over East Asia during the summer over the Yangtze-Huaihe River Basins, resulting in large socio-economic losses in many countries. Because these two extremes of monsoonal climate are very different, with significant social, economic, and environmental impacts, simulating strong and weak EASMs with high accuracy is important. Consequently, we investigated how HRA

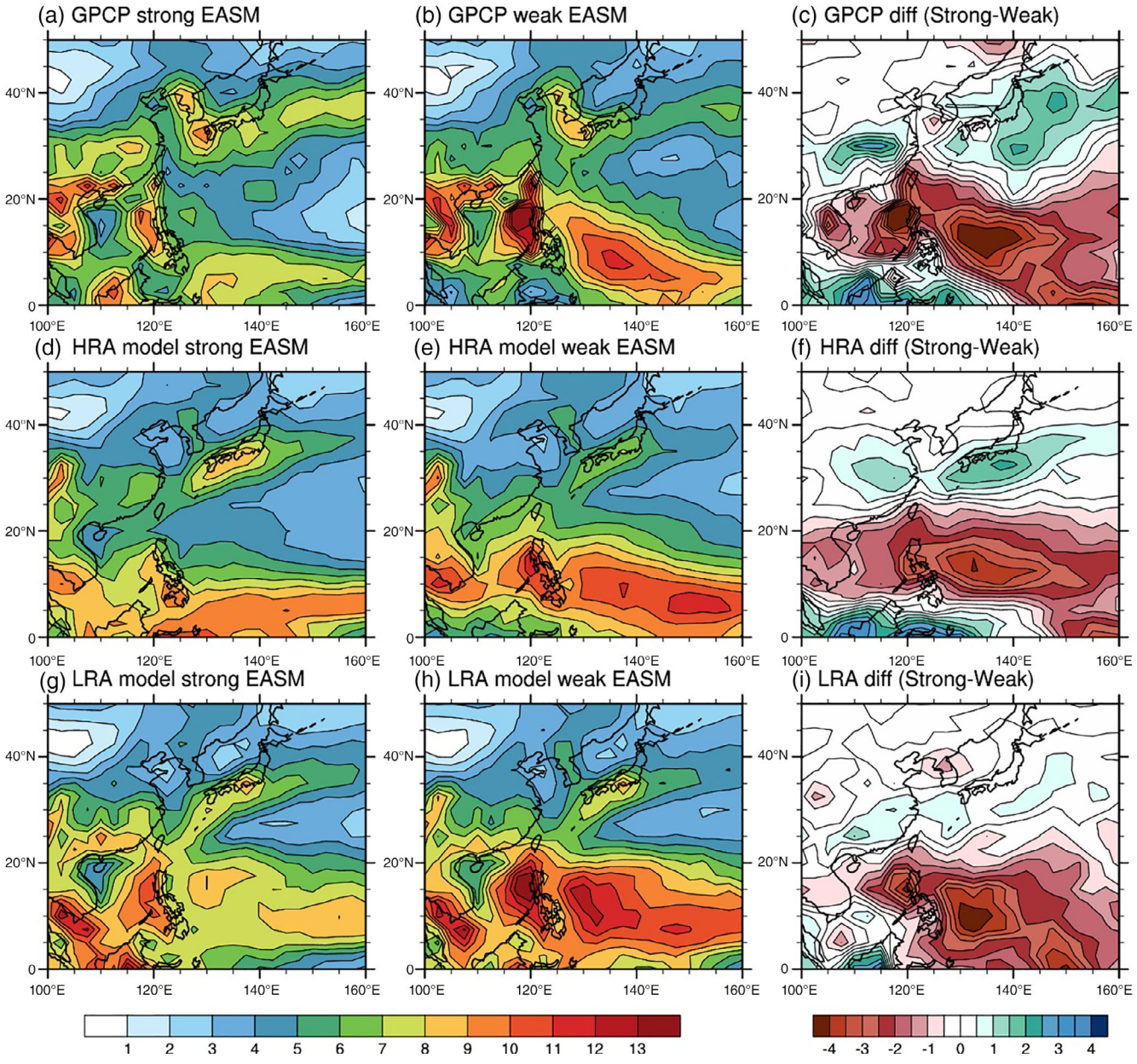

FIGURE 5 Composite map of summer mean (JJA) precipitation for (a, d, g) strong, (b, e, h) weak EASM years and (c, f, i) difference between strong and weak EASM years from the (a, b, c) observation, (d, e, f) CMIP5 HRA model ensemble and (g, h, i) CMIP5 LRA model ensemble [Colour figure can be viewed at wileyonlinelibrary.com]

and LRA CMIP5 models for air–sea interactions performed in their simulations of extreme monsoon years. Extreme EASM years were selected based on the Western North Pacific Monsoon Index (WNPMI) (Wang and Fan, 1999; Wang *et al*., 2001). As the phase of the WNPSM is inter-annually opposite to that of the EASM, WNPMI has been considered as a qualified index for the EASM as well (Kwon *et al*., 2005; Cha *et al*., 2011). Strong (weak) EASM years are defined as years as WNPMI below −0.75 σ (above +0.75 σ). As a result, five strong (1983, 1988, 1995, 1996, 1998) and seven weak EASM years (1981, 1982, 1984, 1985 1986, 1990, 1994) were selected from the observational data set. Strong and weak EASM years in HRA and LRA models were also divided using the simulated WNPMI (Table 3).

Figure 4 is a Taylor diagram showing the pattern correlations and *SD* of precipitation from ensembles of CMIP5 models for the period of strong EASM years and weak EASM year. HRA models simulating more realistic ASI tended to have higher pattern correlation with observed precipitation in both period of EASM years. Furthermore, the standard deviation of most HRA models was closer to the observations than that of LRA models as well. The performance of the ensemble of HRA models was better than that of the ensemble of LRA models in terms of spatial distribution and variance of precipitation. The pattern correlation coefficient of summer precipitation for strong EASM periods in the ensemble of HRA models (0.72) was higher than those in the ensemble of LRA models (0.64) and the *SD* in the ensemble of HRA models was almost the same as that of the observations, whereas that in the ensemble of LRA models was 1.1 times larger than that of the observations. As with strong EASM periods, the pattern correlation coefficient of summer precipitation and the *SD* was higher in the ensemble of HRA models (0.81, 1.04) than those in the ensemble of LRA models (0.77, 1.2) for weak EASM periods.

Summer mean (JJA) precipitation was significantly different between strong and weak EASM years (Figure 5). The EASM clearly originated in central China, Korea, and Japan in the strong EASM years (Figure 5a), while the WNPSM was much weaker than the weak EASM years climatology (Not shown). In weak EASM years, however, the EASM was much weaker, and the WNPSM was much stronger than in strong EASM years (Figure 5b). The rate of rainfall around eastern China and southern Japan was particularly altered (Figure 5c). These different aspects were reasonably reproduced with the ensemble of CMIP5 HRA models (Figure 5d–f). Although overall rainfall intensity was weaker than that observed, the EASM (WNPSM) rainband was noticeably stronger (weaker) in strong EASM years than in weak EASM years. LRA models also clearly reproduced the change in WNPSM precipitation intensity. Weak EASM years have a much stronger WNPSM rainband than years with a strong EASM. However, the spatial distribution and rate of rainfall of the EASM were nearly the same across extreme EASM years (Figure 5g–i). On the contrary, the rate of rainfall on the Korean peninsula was unreasonably higher in years with a weak EASM than in years with a strong EASM. The HRA model ensemble's performance was better than the LRA model ensemble's skill in both extreme EASM years (Table 4).

To clarify the relationship between ASI and the extreme EASM simulations, the biases of difference in summer mean precipitation between the strong and weak EASM years over the northeast Asia summer monsoon (NEASM) area was analyzed (Figure 6). While the HRA models had a bias within ±0.3, the LRA models had a larger bias than HRA models except for two models. The exceptive two models in the LRA models showed that the bias in the difference of summer precipitation between extreme EASM years was close to the observation, but a flaw was found in reproducing more overall

TABLE 4 RMSE and bias of precipitation for strong and weak EASM between the observation and simulations of CMIP5 HRA and LRA model ensembles

	HRA model ensemble		LRA model ensemble	
	RMSE	Bias	RMSE	Bias
Strong EASM	1.63	0.12	1.95	0.37
Weak EASM	1.58	0.12	1.97	0.59

Note: Statistics are calculated for the area between 0–50°N and 100–160°E.

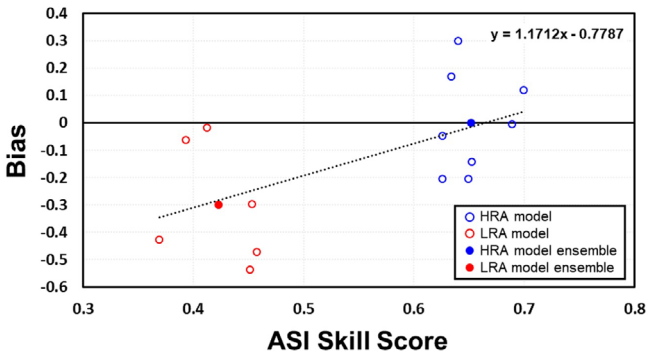

FIGURE 6 Scatter plot of ASI and biases of difference in summer mean precipitation between strong and weak EASM years over the Northeast Asia summer monsoon (NEASM) area. Black dotted line indicates the regression line among models. The NEASM area is defined as 30–50°N and 110–145°E based on Lee *et al*. (2005) [Colour figure can be viewed at wileyonlinelibrary.com]

mid-latitude precipitation, especially inland China, than observation during extreme EASM years. The performance of the ensemble of HRA models was better than that of the ensemble of LRA models in terms of bias and ASI. The bias of difference summer precipitation for extreme EASM years in the ensemble HRA models was almost the same as that of the observations, whereas that in the ensemble of LRA model had a large bias (−0.3) and ASI skill score in the ensemble of HRA models (0.65) was higher those in the ensemble of LRA models (0.42). Thus, model ensembles with poor ASI cannot reasonably reproduce seasonal mean precipitation over the NEASM area for the extreme EASM years, indicating low ability to simulate the interannal variability of the EASM.

Precipitation for the extreme EASM years is affected by location and strength of the WNPSH (Chang *et al*., 2000; Lu, 2001; Lee *et al*., 2005; Zhou *et al*., 2009; Song and Zhou, 2015). To examine the reason for the poor performance of LRA models in simulating extreme EASM, the synoptic fields for the strong and weak EASM years in R-2 reanalysis data, using HRA and LRA models were also analyzed (Figure 7). In strong EASM years

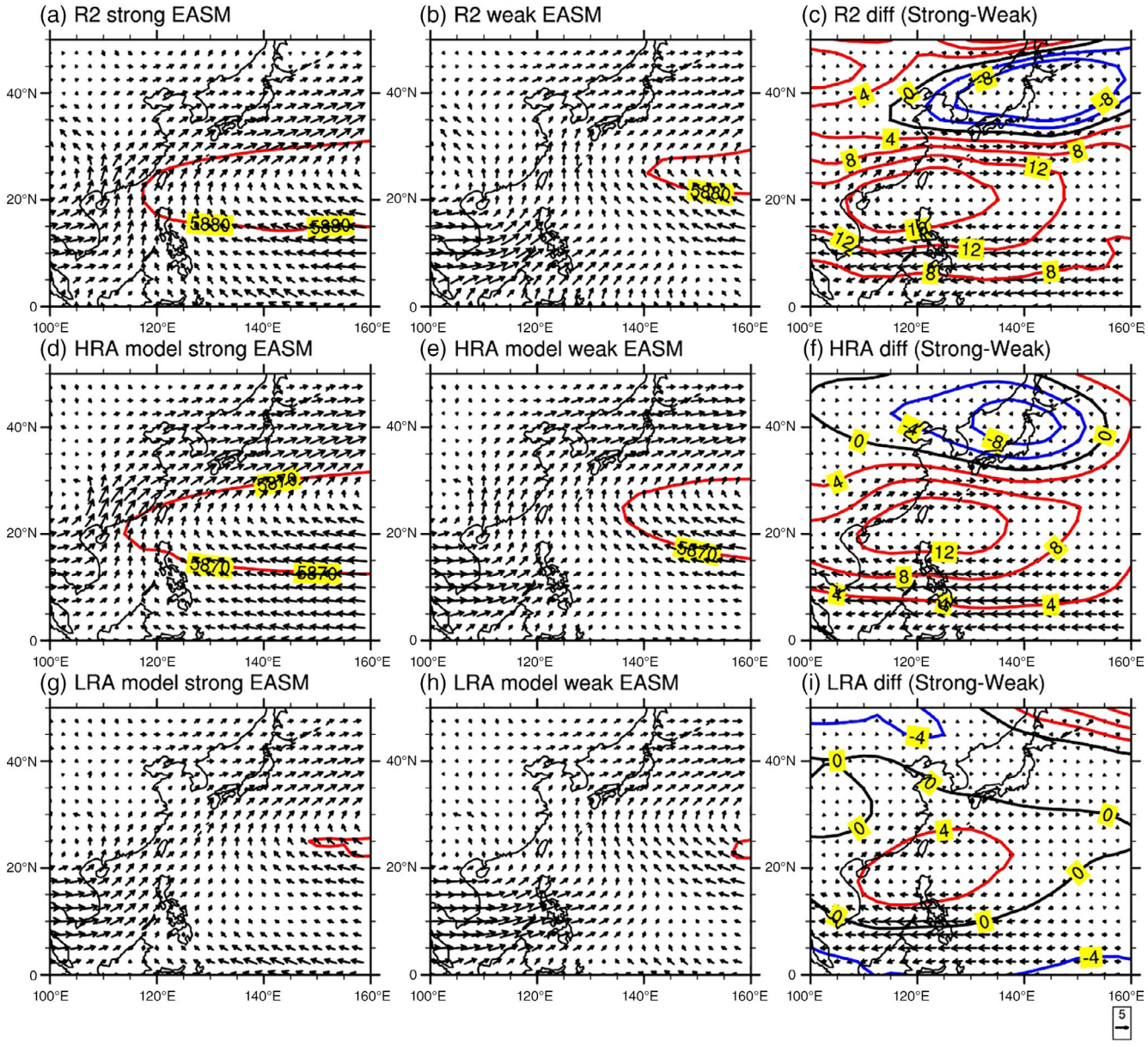

FIGURE 7 Composite map of summer mean (JJA) wind at 850 hPa (vector; units; $m \cdot s^{-1}$) and geopotential height at 500 hPa (+: Red line; −: Blue line; units; gpm) for (a, d, g) strong, (b, e, h) weak EASM years and (c, f, i) difference between strong and weak EASM years from the (a, b, c) reanalysis, (d, e, f) CMIP5 HRA model ensemble and (g, h, i) CMIP5 LRA model ensemble [Colour figure can be viewed at wileyonlinelibrary.com]

(Figure 7a), the low-level southwesterly over East Asia was stronger, and the WNPSH, represented by the 5,880 gpm contour line, expanded further to the west, compared with the weak EASM years. The wind could transport more moist air including large quantities of water vapour northward along the western edge of the WNPSH from the eastern Indian Ocean and tropical Pacific Ocean to the mid-latitudes over East Asia, which led to a strong EASM and increased precipitation. In contrast, the strengthened WNPSH, coexisting with the weak westerly into the tropical WNP, was associated with reduced precipitation over South-East Asia and the subtropical WNP. In weak EASM years (Figure 7b), the low-level westerly from the Indian Ocean to the WNP was reasonably strong and the WNPSH was shifted eastward compared with the strong EASM years. This weakened WNPSH could result in intensified low-level winds from the Indian Ocean to the subtropical WNP and reduced northward winds from the tropics to East Asian countries (i.e., China, Korea, and Japan). In weak EASM years, therefore, precipitation in low (mid-) latitudes increased (decreased) relative to the strong EASM years, indicating a strong WNPSM. HRA models reasonably reproduced these differences between years of strong and weak EASM (Figure 7d–f). The ensemble of HRA models in strong EASM years reproduced realistic geopotential height and low-level circulation, allowing sufficient moisture transport into mid-latitudes. Consequently, the EASM rainband was sufficiently developed. The synoptic field of the ensemble of HRA models in weak EASM years was also similar to the observations. The shift in the 500-hPa geopotential height demonstrated that the WNPSH was much weaker than that in strong EASM years, and anticyclonic circulation over the WNP was also shifted rightward. More westerly winds occurred into the WNPSM region, rather than into the EASM region. In contrast, the ensemble of LRA models reproduced distorted synoptic-scale atmospheric conditions in both extreme EASM years (Figure 7g–i). The WNPSH, which should be located over East Asia and WNP, was not apparent in the strong EASM years; the WNPSH also shrank eastward compared with observed data. This weakened WNPSH could result in intensified low-level winds from the Indian Ocean to the subtropical WNP and reduced northward winds from subtropical to mid-latitudes. For example, Cha *et al.* (2008) and Cha and Lee (2009) demonstrated that these synoptic conditions might induce an overestimation of precipitation over the WNPSM region due to the uncoupled air–sea interactions. The strengthened low-level westerly extended to the subtropical WNP, enhancing latent heat flux from the sea surface, by increasing planetary boundary layer mechanical mixing in models. Convective available potential energy increased due to the enhanced surface latent heat flux; more active convection and overestimated precipitation are then expected to follow. Due to low-level southwesterly winds into the mid-latitudes were also much underestimated, precipitation was concentrated in the lower latitudes, and it was difficult to reproduce the EASM in the mid-latitudes. In weak EASM years, westerlies from the eastern Indian Ocean into the WNP were much exaggerated, which may cause a large increase in rainfall over the SCS and the Philippines Sea. Although there were quite reasonable differences associated with the WNPSM, the circulation over the EASM region was little changed. This result clearly demonstrated the difference between the abilities of HRA and LRA models to perform accurate simulations of EASM/WNPSM rainfall and synoptic fields in extreme EASM years. The HRA model ensemble with realistic ASI better simulated the differences of feature between strong and weak EASM, whereas the LRA model ensemble did not.

4 | SUMMARY AND CONCLUSION

This study examined the performance of global climate models in reproducing the extreme EASM and demonstrated that good and poor performing models differ according to their ability to accurately simulate air–sea interactions over the WNP. The relationship between precipitation and SST (ASI) over the WNP is different from those over other basins at the same latitude; ASI over the WNP demonstrates the dominance of the forcing of atmosphere onto ocean unlike other basins. These characteristics are not realistically simulated in atmospheric-only models, which use a prescribed SST. This flaw is expected to be improved in models that reasonably simulate atmosphere–ocean interactions. To examine whether a realistic simulation of atmosphere–ocean interactions overcomes this problem, the evaluation, and intercomparison of CMIP3 and CMIP5 ensembles were performed, assessing their performance in simulating the WNP air–sea interaction. The overall performance in simulating negative ASI over the WNP was improved for CMIP5 models compared with CMIP3 models. In particular, in CMIP5 HRA models, stronger negative signals over the WNP were indicated, implying that atmospheric forcing on the ocean was realistically simulated.

The impact of simulations of air–sea interactions on the performance of simulation of the extreme EASM was also analyzed using the CMIP5 model data. In HRA models, a realistic ASI was reproduced, demonstrating the negative correlation between precipitation and SST over the SCS and the Philippine Sea. The spatial

distribution of monsoon precipitation was also relatively well captured in HRA models. In HRA models, the distribution of summer precipitation in extreme EASM years, which is divided into the EASM and WNPSM, was realistically simulated, whereas LRA models tended to overestimate the overall domain. Differences in the WNPSM between the strong and weak EASM years were captured by both HRA and LRA models. However, only CMIP5 HRA models, with realistic representations of the ASI, were effective at simulating the extreme EASM. The location of the rainband and intensity of the extreme EASM were much closer to the observed values, while the ensemble of LRA models could not capture the difference between strong and weak EASM years. The synoptic field analysis demonstrated that the WNPSH was well developed in HRA models, and low-level winds were also adequately simulated for extreme EASM years. In LRA models, however, the extreme EASM was not reasonably reproduced because low-level westerly winds were overestimated, and water vapour was not transported to the mid-latitudes because the simulated WNPSH was significantly weakened.

It is concluded that GCMs have different capacities to reasonably simulate the extreme EASM because of the differences in their ability to accurately simulate air–sea interactions in the WNP. In particular, defects in the simulation of the relationship between atmosphere and ocean over the WNP contribute to the inability of GCMs to properly reproduce the extreme EASM. Therefore, models that realistically simulate physical processes between the atmosphere and ocean are needed to realistically reproduce the spatial and temporal distribution of the EASM.

The fundamental causes of differences in quality of the simulations of air–sea interactions over the WNP by CMIP5 models were not addressed in this study. To overcome this limitation, the physical characteristics and sensitivities of the models among internal variables need to be further identified. In addition, the bias compensation concept that the cold SST bias of the coupled model can suppress the precipitation and improve the precipitation simulation proposed by Song and Zhou (2014b) and Yang *et al*. (2019) was not considered in this research. Based on the bias compensation, the improvement of the atmospheric model can also lead to improved simulation of the EASM because the better atmospheric model has less benefit from the bias compensation and produce much less SST bias in the coupled model. Therefore, further researches on the quantitative analysis of the impacts of air–sea interaction and atmospheric model improvement on the EASM simulation remains challenging. It is also needed to investigate the performance of recent CMIP6 models to simulate air–sea interaction and its impact on the simulation of the EASM.

ACKNOWLEDGEMENTS

This work was funded by the Korea Meteorological Administration Research and Development Program under Grant KMI (KMI2020-01412).

ORCID

Dong-Hyun Cha https://orcid.org/0000-0001-5053-6741
Kyong-Hwan Seo https://orcid.org/0000-0001-6305-5488

REFERENCES

Adler, R.F., Huffman, G.J., Chang, A., Ferraro, R., Xie, P.-P., Janowiak, J., Rudolf, B., Schneider, U., Curtis, S. and Bolvin, D. (2003) The version-2 global precipitation climatology project (GPCP) monthly precipitation analysis (1979–present). *Journal of Hydrometeorology*, 4, 1147–1167.

Cha, D.-H., Jin, C.-S. and Lee, D.-K. (2011) Impact of local sea surface temperature anomaly over the western North Pacific on extreme east Asian summer monsoon. *Climate Dynamics*, 37, 1691–1705.

Cha, D.-H., Jin, C.-S., Moon, J.-H. and Lee, D.-K. (2016) Improvement of regional climate simulation of east Asian summer monsoon by coupled air–sea interaction and large-scale nudging. *International Journal of Climatology*, 36, 334–345.

Cha, D.-H. and Lee, D.-K. (2009) Reduction of systematic errors in regional climate simulations of the summer monsoon over East Asia and the western North Pacific by applying the spectral nudging technique. *Journal of Geophysical Research-Atmospheres*, 114, D14108.

Cha, D.-H., Lee, D.-K. and Hong, S.-Y. (2008) Impact of boundary layer processes on seasonal simulation of the East Asian summer monsoon using a regional climate model. *Meteorology and Atmospheric Physics*, 100, 53–72.

Chang, C., Zhang, Y. and Li, T. (2000) Interannual and interdecadal variations of the east Asian summer monsoon and tropical Pacific SSTs. Part I: roles of the subtropical ridge. *Journal of Climate*, 13, 4310–4325.

Fu, X. and Wang, B. (2004) Differences of boreal summer intraseasonal oscillations simulated in an atmosphere–ocean coupled model and an atmosphere-only model. *Journal of Climate*, 17, 1263–1271.

Fu, X., Wang, B. and Li, T. (2002) Impacts of air–sea coupling on the simulation of mean Asian summer monsoon in the ECHAM4 model. *Monthly Weather Review*, 130, 2889–2904.

Gadgil, S. and Sajani, S. (1998) Monsoon precipitation in the AMIP runs. *Climate Dynamics*, 14, 659–689.

Huang, B., Thorne, P.W., Banzon, V.F., Boyer, T., Chepurin, G., Lawrimore, J.H., Menne, M.J., Smith, T.M., Vose, R.S. and Zhang, H.-M. (2017) Extended reconstructed sea surface temperature, version 5 (ERSSTv5): upgrades, validations, and intercomparisons. *Journal of Climate*, 30, 8179–8205.

Kanamitsu, M., Ebisuzaki, W., Woollen, J., Yang, S.-K., Hnilo, J., Fiorino, M. and Potter, G. (2002) NCEP–DOE AMIP-II reanalysis (R-2). *Bulletin of the American Meteorological Society*, 83, 1631–1644.

Kim, E.J. and Hong, S.Y. (2010) Impact of air-sea interaction on east Asian summer monsoon climate in WRF. *Journal of Geophysical Research-Atmospheres*, 115, D19118.

Kwon, M., Jhun, J.G., Wang, B., An, S.I. and Kug, J.S. (2005) Decadal change in relationship between east Asian and WNP summer monsoons. *Geophysical Research Letters*, 32, L16709.

Lau, K., Kim, K. and Yang, S. (2000) Dynamical and boundary forcing characteristics of regional components of the Asian summer monsoon. *Journal of Climate*, 13, 2461–2482.

Lee, E.-J., Jhun, J.-G. and Park, C.-K. (2005) Remote connection of the northeast Asian summer rainfall variation revealed by a newly defined monsoon index. *Journal of Climate*, 18, 4381–4393.

Lu, R. (2001) Interannual variability of the summertime North Pacific subtropical high and its relation to atmospheric convection over the warm pool. *Journal of the Meteorological Society of Japan. Ser. II*, 79, 771–783.

Lu, R. and Lu, S. (2014) Local and remote factors affecting the SST–precipitation relationship over the western North Pacific during summer. *Journal of Climate*, 27, 5132–5147.

Meehl, G.A., Boer, G.J., Covey, C., Latif, M. and Stouffer, R.J. (2000) The coupled model intercomparison project (CMIP). *Bulletin of the American Meteorological Society*, 81, 313–318.

Meehl, G.A., Covey, C., Delworth, T., Latif, M., McAvaney, B., Mitchell, J.F., Stouffer, R.J. and Taylor, K.E. (2007) The WCRP CMIP3 multi-model dataset: a new era in climate change research. *Bulletin of the American Meteorological Society*, 88, 1383–1394.

Park, C.-K. and Schubert, S.D. (1997) On the nature of the 1994 East Asian summer drought. *Journal of Climate*, 10, 1056–1070.

Seo, K.-H., Ok, J., Son, J.-H. and Cha, D.-H. (2013) Assessing future changes in the east Asian summer monsoon using CMIP5 coupled models. *Journal of Climate*, 26, 7662–7675.

Seo, K.-H., Schemm, J.-K.E., Wang, W. and Kumar, A. (2007) The boreal summer intraseasonal oscillation simulated in the NCEP climate forecast system: the effect of sea surface temperature. *Monthly Weather Review*, 135, 1807–1827.

Son, J.H., Seo, K.H. and Wang, B. (2019) Dynamical control of the Tibetan plateau on the east Asian summer monsoon. *Geophysical Research Letters*, 46, 7672–7679.

Song, F. and Zhou, T. (2014a) Inter-annual variability of east Asian summer monsoon simulated by CMIP3 and CMIP5 AGCMs: skill dependence on Indian Ocean-western Pacific anticyclone teleconnection. *Journal of Climate*, 27, 1679–1697.

Song, F. and Zhou, T. (2014b) The climatology and inter-annual variability of east Asian summer monsoon in CMIP5 coupled models: does air-sea coupling improve the simulations? *Journal of Climate*, 27, 8761–8777.

Song, F. and Zhou, T. (2015) The dominant role of internal variability in modulating the decadal variation of the east Asian summer monsoon–ENSO relationship during the 20th century. *Journal of Climate*, 28, 7093–7107.

Taylor, K.E. (2001) Summarizing multiple aspects of model performance in a single diagram. *Journal of Geophysical Research-Atmospheres*, 106, 7183–7192.

Taylor, K.E., Stouffer, R.J. and Meehl, G.A. (2012) An overview of CMIP5 and the experiment design. *Bulletin of the American Meteorological Society*, 93, 485–498.

Tompkins, A.M. (2001) On the relationship between tropical convection and sea surface temperature. *Journal of Climate*, 14, 633–637.

Wang, B., Ding, Q., Fu, X., Kang, I.S., Jin, K., Shukla, J. and Doblas-Reyes, F. (2005) Fundamental challenge in simulation and prediction of summer monsoon rainfall. *Geophysical Research Letters*, 32, L15711.

Wang, B. and Fan, Z. (1999) Choice of south Asian summer monsoon indices. *Bulletin of the American Meteorological Society*, 80, 629–638.

Wang, B. and LinHo. (2002) Rainy season of the Asian–Pacific summer monsoon. *Journal of Climate*, 15, 386–398.

Wang, B., Wu, R. and Lau, K. (2001) Interannual variability of the Asian summer monsoon: contrasts between the Indian and the western North Pacific–east Asian monsoons. *Journal of Climate*, 14, 4073–4090.

Wu, G., Liu, Y., He, B., Bao, Q., Duan, A. and Jin, F.-F. (2012) Thermal controls on the Asian summer monsoon. *Scientific Reports*, 2, 404.

Yang, B., Zhang, Y., Qian, Y., Song, F., Leung, L.R., Wu, P., Guo, Z., Lu, Y. and Huang, A. (2019) Better monsoon precipitation in coupled climate models due to bias compensation. *NPJ Climate and Atmospheric Science*, 2(1), 1–8.

Yim, S.-Y., Yeh, S.-W., Wu, R. and Jhun, J.-G. (2008) The influence of ENSO on decadal variations in the relationship between the east Asian and western North Pacific summer monsoons. *Journal of Climate*, 21, 3165–3179.

Zhou, T., Yu, R., Zhang, J., Drange, H., Cassou, C., Deser, C., Hodson, D., Sanchez-Gomez, E., Li, J., Keenlyside, N., Xin, X. and Okumura, Y. (2009) Why the western Pacific subtropical high has extended westward since the late 1970s. *Journal of Climate*, 22(8), 2199–2215.

Zou, L. and Zhou, T. (2013) Can a Regional Ocean-atmosphere coupled model improve the simulation of the interannual variability of the Western North Pacific summer monsoon? *Journal of Climate*, 26, 2353–2367.

Zou, L. and Zhou, T. (2014) Simulation of the western North Pacific summer monsoon by regional ocean-atmosphere coupled model: impacts of oceanic components. *Chinese Science Bulletin*, 59(7), 662–673.

Zou, L., Zhou, T. and Peng, D. (2016) Dynamical downscaling of historical climate over CORDEX East Asia domain: a comparison of regional ocean-atmosphere coupled model to stand-alone RCM simulations. *Journal of Geophysical Research-Atmospheres*, 121(4), 1442–1458.

How to cite this article: Kim, T., Lee, S., Park, H.-J., Cha, D.-H., & Seo, K.-H. (2021). The impact of coupled air–sea interaction on extreme East Asian summer monsoon simulation in CMIP5 models. *International Journal of Climatology*, 1–14. https://doi.org/10.1002/joc.7198